MIPR No. 1-01182
AMCMS Code: 5910.21.63389
HDL Proj: E01E4

HDL-TR-1599

MAGNETIC FIELDS INSIDE MISSILE CELL-LIKE STRUCTURES

by

Daniel J. Spohn

July 1972

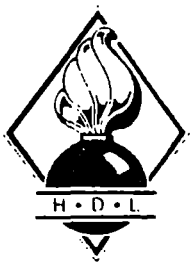

U.S. ARMY MATERIEL COMMAND
HARRY DIAMOND LABORATORIES
WASHINGTON, D.C. 20438

ABSTRACT

The analytical work of Latham and Lee describing the static magnetic field inside idealized structures resembling missile cells was reviewed, and a CALCOMP plotting routine was used to graph the results. These results were experimentally verified using a pulsed, parallel-plate transmission line.

ACKNOWLEDGMENT

This work was sponsored by the Safeguard Systems Command (SAFSCOM) for the Safeguard EMP program. The author wishes to thank Dr. John Bombardt for his guidance in the analytical review and Forrest Gunnison for his assistance with the instrumentation for the experimental verification.

CONTENTS

TABLES

FIGURES

1. INTRODUCTION

From an EMP standpoint, the behavior of electromagnetic fields inside missile cells must be understood for an effective hardening program. Other related work was reviewed, and that work was extended to provide graphic and numerical results to supplement the published analytical expressions. An experiment was designed to verify the analytical results.

2. MAGNETIC FIELD CALCULATIONS

The magnetic fields inside several idealized structures resembling missile cells were investigated under a contract to the Air Force by R.W. Latham and K.S.H. Lee.[1] The idealized structures assumed for the purposes of calculation were (fig. 1): (1) a perfectly conducting, semi-infinite cylinder with an infinite, perfectly conducting flange; (2) a perfectly conducting, semi-infinite cylinder; (3) a semi-infinite, perfectly conducting, flanged cylinder with a resistive cap; and (4) a semi-infinite, perfectly conducting, flanged cylinder with a perfectly conducting cap separated from the cylinder by an annular slot. They assumed that quasi-static conditions apply; i.e., the magnetic field can be considered separately from the electric field and the field can be treated by using scalar potentials. The waveshape of the internal field is assumed to be obtained from the external field by a linear scaling process.

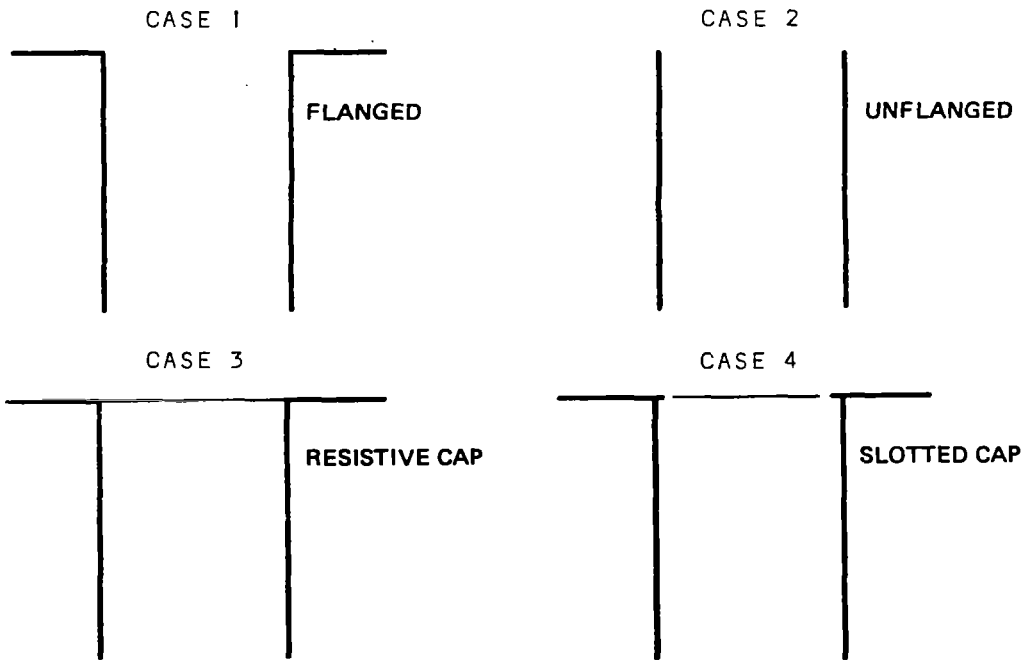

Figure 1. Latham & Lee geometries.

[1] Latham, R.W. and Lee, K.S.H., "A Study of Fields of a Semi-Infinite Pipe Exposed to a Low-Frequency Magnetic Field," EMP Interaction Note X, AFWL, August 1967.

Their calculations indicate that the magnetic field inside the various structures is related to the external field by the equation

$$B_x = \frac{1}{2} C_1 B_0 \exp(\xi_1 z/a) \qquad (1)$$

where $\frac{1}{2} C_1$ is a constant defined in table I and

B_x = the radial component of the field with $\phi = 0$ and $r = 0$

B_0 = external field (perpendicular to the axis of the cylinder with $\phi = 0$)

ξ_1 = 1.84118

a = radius of the cylinder.

Table I. Values of $\frac{1}{2}C_1$ in eq (1) for structures shown in figure 1.

Case	Structure	$\frac{1}{2}C_1$
1	Flanged cylinder	0.838
2	Cylinder only	1.120
3	Flanged cylinder with resistive cap	$0.838/[1 - i(0.349\omega/\omega_0)]$
4	Flanged cylinder with slotted, 1/2304 radius wide at a distance from the wall of:	
	1/10 radius	0.303
	1/72 radius	0.335

Further review of their work indicated that an expression could be obtained for the field magnitude anywhere inside the cylinders. The expressions for the fields inside the various structures are in spherical coordinates.

Flanged Cylinder (fig. 2 and 3)

$$\begin{aligned}\overline{B} = {} & \overline{u}_\rho\{(C_1/\xi_1)B_0 a(\cos\phi)[(\xi_1/a)J_0(\xi_1\rho/a) - (1/\rho)J_1(\xi_1\rho/a)]\exp(\xi_1 z/a)\} \\ & + \overline{u}_\phi\{-C_1/(\xi_1\rho)B_0 a(\sin\phi)J_1(\xi_1\rho/a)\exp(\xi_1 z/a)\} \\ & + \overline{u}_z\{C_1 B_0(\cos\phi)J_1(\xi_1\rho/a)\exp(\xi_1 z/a)\} \qquad (2)\end{aligned}$$

where

C_1 = 1.676

ξ_1 = 1.84118

$\overline{u}$ = unit vector

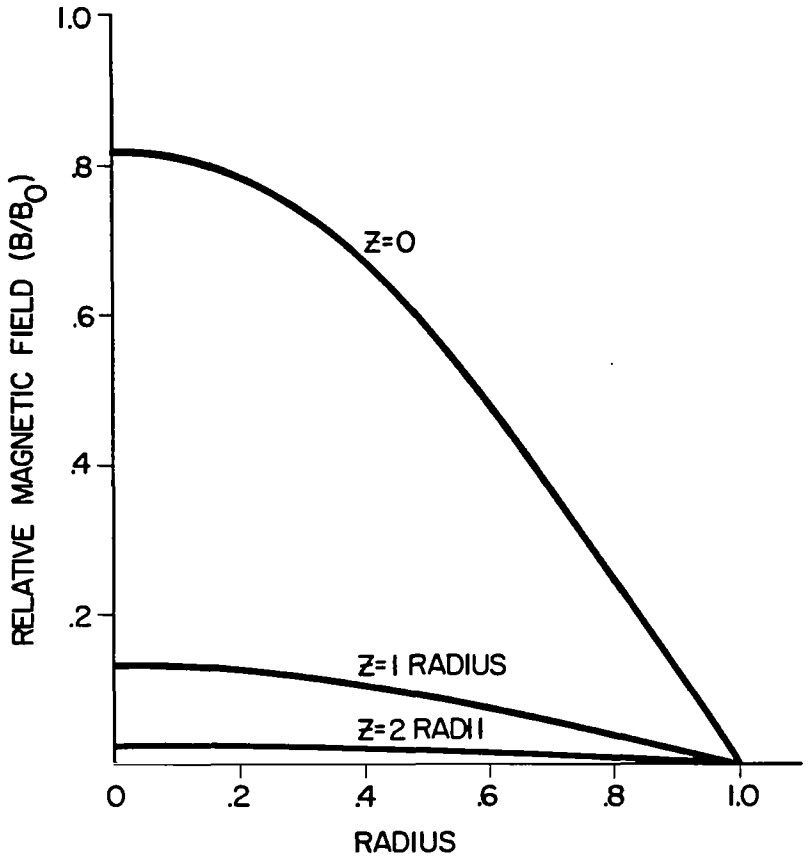

Figure 2. Case 1: flanged cylinder, B_r versus r at $\phi = 0$.

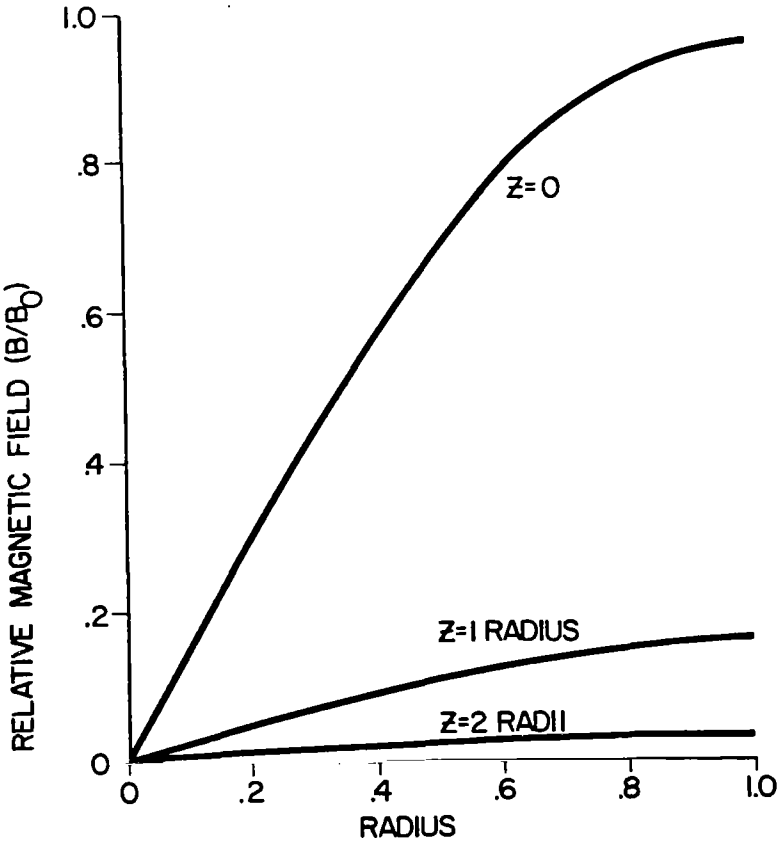

Figure 3. Case 1: flanged cylinder, B_Z versus r at $\phi = 0$.

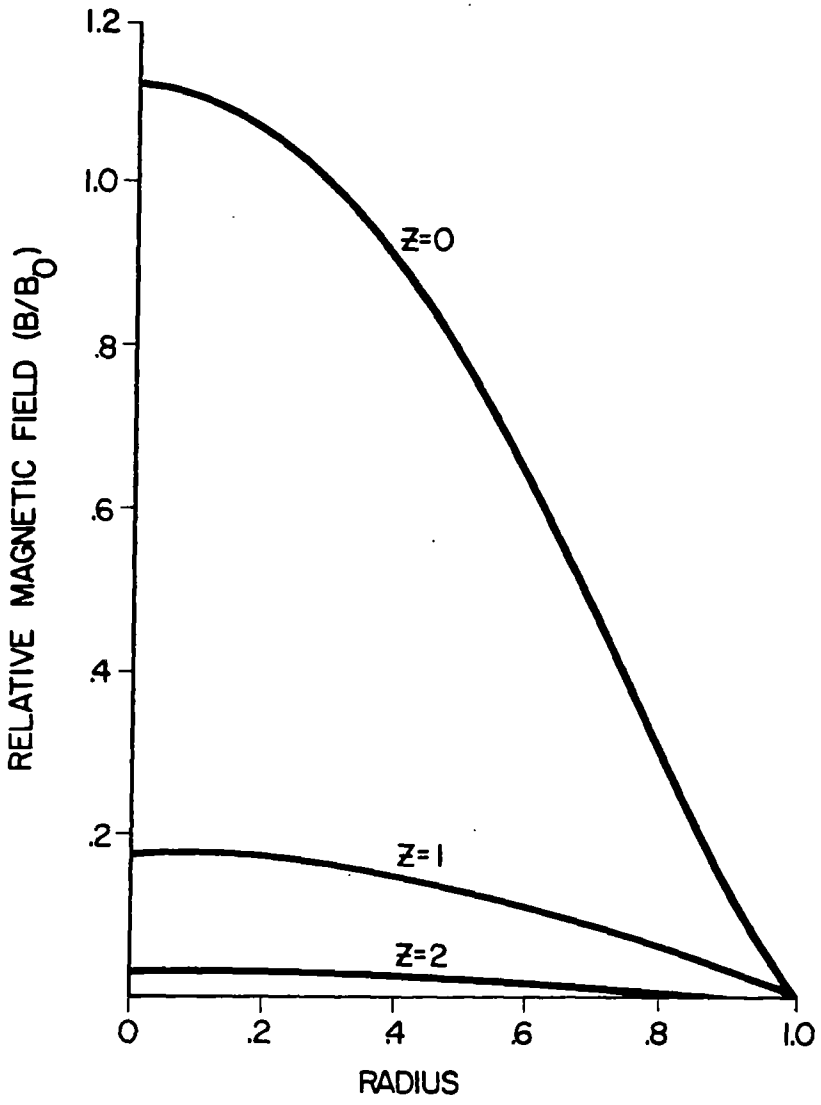

Figure 4. Case 2: unflanged cylinder, B_r versus r at $\phi = 0$.

Unflanged Cylinder (fig. 4 and 5)

$$\overline{B} = \overline{u}_\rho\{B_0(C_1/2)\cos\phi[J_0(\xi_1\rho/a) - J_2(\xi_1\rho/a)]\exp(\xi_1 z/a)\}$$
$$+ \overline{u}_\phi\{-B_0C_1a/(\rho\xi_1)\sin\phi[J_1(\xi_1\rho/a)]\exp(\xi_1 z/a)\}$$
$$+ \overline{u}_z\{B_0C_1\cos\phi[J_1(\xi_1\rho/a)]\exp(\xi_1 z/a)\} \qquad (3)$$

where $C_1 = 2.240$

$\xi_1 = 1.84118$

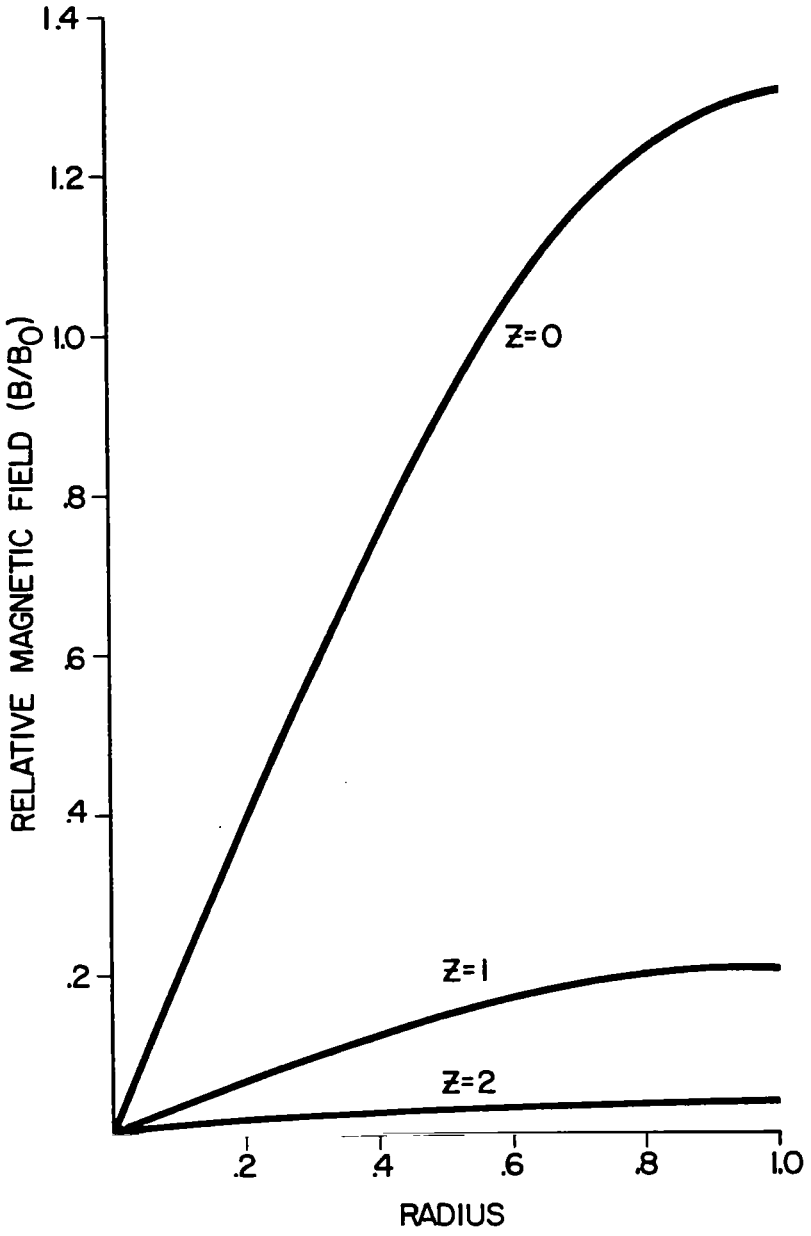

Figure 5. Case 2: unflanged cylinder, B_Z versus r at $\phi = 0$.

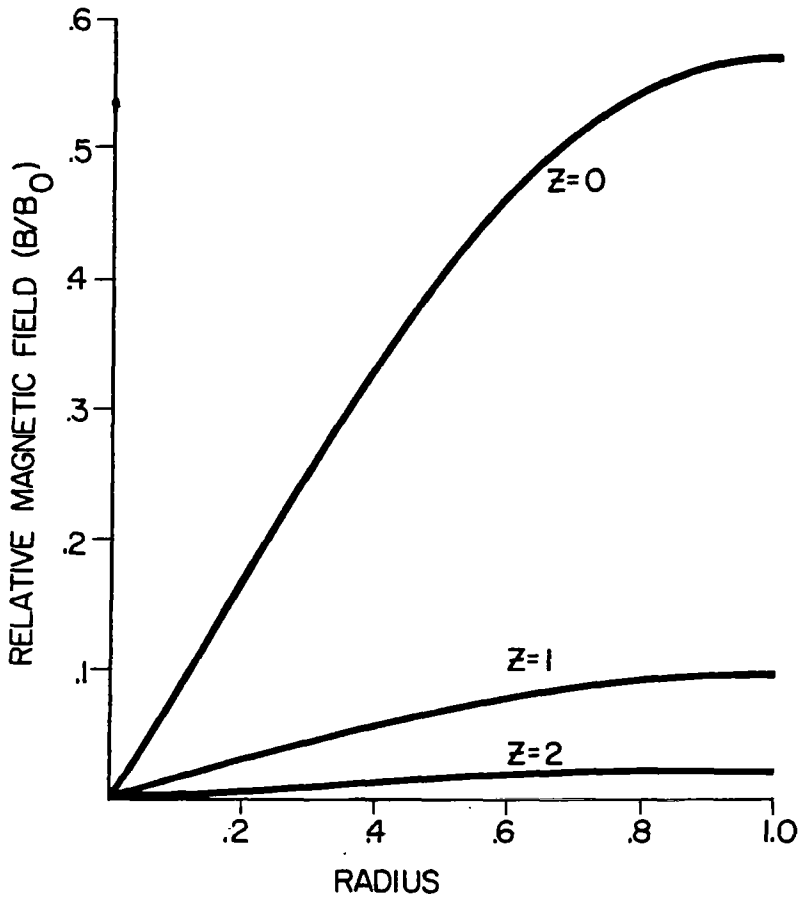

Figure 6. Case 3: resistive cap, $\sigma = 10^{-2}$ ℧/m, B_r versus r at $\phi = 0$.

Resistive Cap (fig. 6 and 7)

$$\vec{B} = \bar{u}_\rho\{(C_1/\xi_1)B_0 a\cos\phi[(\xi_1/a)J_0(\xi_1\rho/a) - (1/\rho)J_1(\xi_1\rho/a)\exp(\xi_1 z/a)\}$$
$$+ \bar{u}_\phi\{-C_1B_0/(\xi_1\rho)a\sin\phi[J_1(\xi_1\rho/a)]\exp(\xi_1 z/a)\}$$
$$+ \bar{u}_z\{C_1B_0\cos\phi[J_1(\xi_1\rho/a)]\exp(\xi_1 z/a)\} \qquad (4)$$

where $\xi_1 = 1.84118$

$$C_1 = \frac{1.6758}{1 - i0.349\frac{\omega}{\omega_0}}$$

ω = frequency

$$\omega_0 = \frac{1}{\mu_0 a\sigma d}$$

μ_0 = permeability of free space

σ = conductivity of cap

d = thickness of the cap

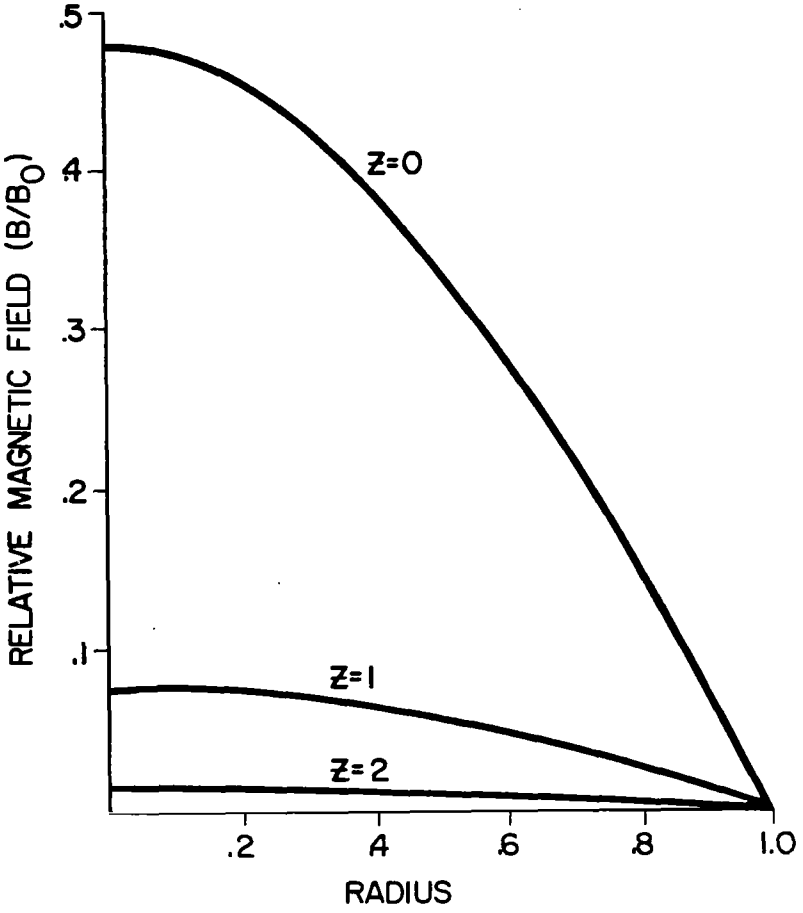

Figure 7. Case 3: resistive cap, $\sigma = 10^{-2}$ ℧/m, B_Z versus r at $\phi = 0$.

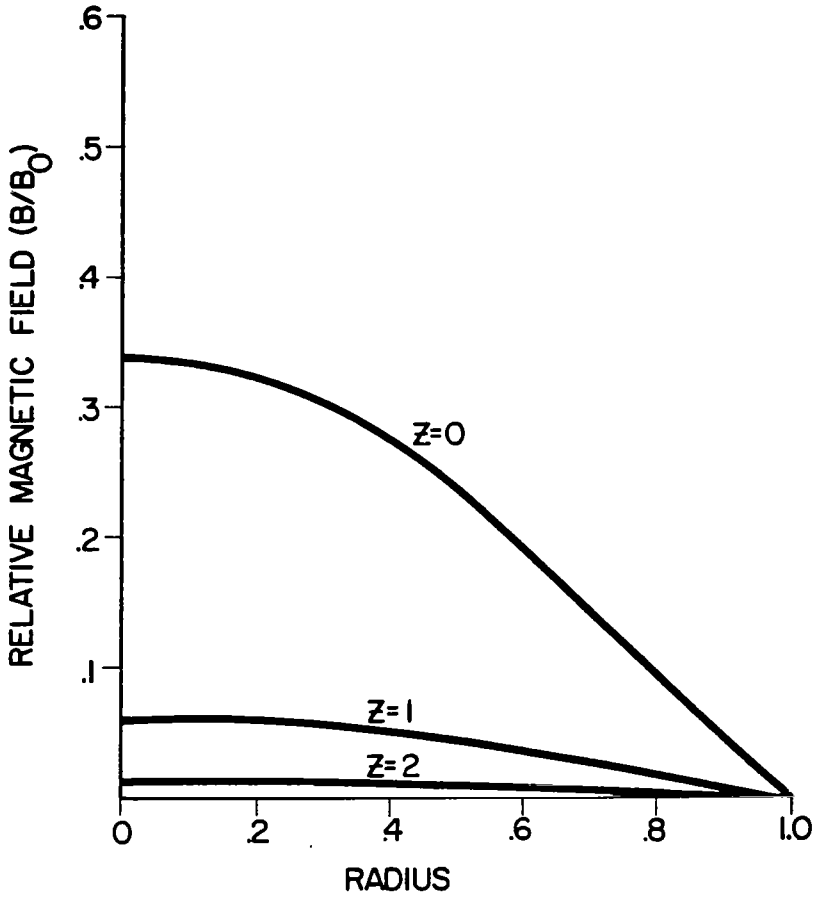

Figure 8. Case 4: slotted top, B_r versus r at $\phi = 0$.

Slotted Cap (fig. 8 and 9)

$$\bar{B} = \bar{u}_\rho\{(B_0C_1a/\xi_1)\cos\phi[(1/a)J_0(\xi_1\rho/a) - (1/\rho)J_1(\xi_1\rho/a)]\exp(\xi_1 z/a)\}$$
$$+ \bar{u}_\phi\{(B_0C_1a/\xi_1\rho)\sin\phi[J_1(\xi_1\rho/a)]\exp(\xi_1 z/a)\}$$
$$+ \bar{u}_z\{C_1B_0\cos\phi[J_1(\xi_1\rho/a)]\exp(\xi_1 z/a)\} \qquad (5)$$

where $\xi_1 = 1.84118$

$$C_1 = \frac{\pi\xi_1^2}{(\xi_1^2 - 1)[J_1(\xi_1)]^2} \frac{\bar{x}J_1(\xi_1\bar{x})}{1.46 - \ell n\,\Delta + \ell n\,\bar{x} + \bar{x}K_c(\bar{x})} \qquad (6)$$

with $\bar{x}$ = average radius of slot
Δ = width of slot

$$K_c(\bar{x}) = -\int_0^\infty \frac{K_1'(\lambda)[I'(\lambda\bar{x})]^2 d\lambda}{I_1'(\lambda)} \qquad (7)$$

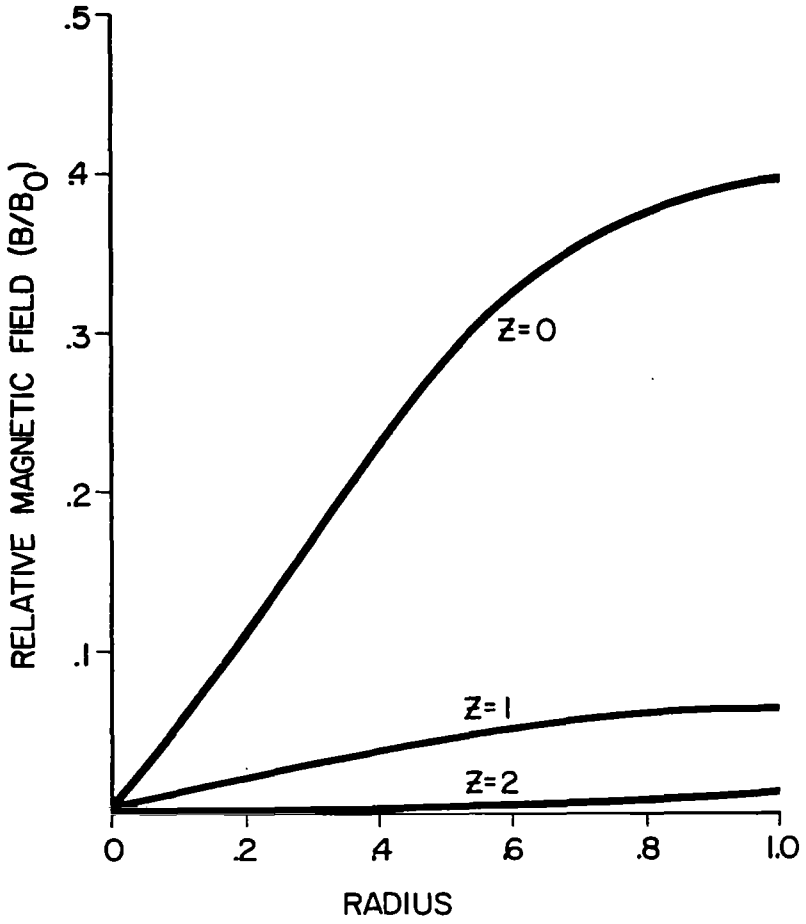

Figure 9. Case 4: slotted top, B_Z versus r at $\phi = 0$.

A computer program was written so that the above results for each of the geometries could be displayed graphically using a CALCOMP routine. On each plot is a family of curves for a particular component at various distances from the top of the cylinder, and in each case, the component of the field is observed along a radius in the direction of the external driving field. Note that all dimensions are normalized, with linear dimensions in terms of the cylinder radius a, and magnetic induction in terms of the assumed external driving field B_0.

3. EXPERIMENTAL VERIFICATION

After the analytical review, several experiments were designed and conducted to verify the magnetic field calculations. The simulator used for these experiments was a parallel-plate transmission line (fig. 10) with dimensions as shown. The pulser driving the line was a capacitor model (built by Physics International Company) and operated at a peak voltage of 50 kV with a risetime of about 15 nsec.

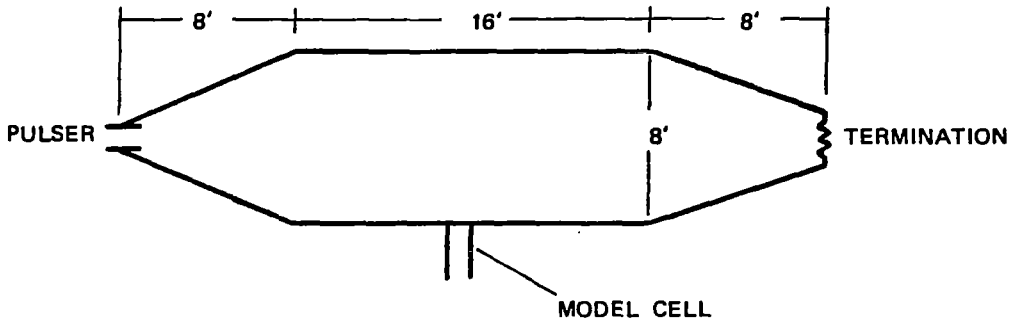

Figure 10. Parallel-plate transmission line.

The model for the cylinder (missile cell) was a 6-in. smoke pipe made of galvanized steel with a galvanized steel flange soldered to it (fig. 11). This was placed through a circular hole in the lower plate of the transmission line and affixed to it with copper conductive tape. To observe the effect of the finite length of the pipe, data were taken using one and two sections of pipe (24 and 48 in.). Data were also taken with the lower end capped to observe the effect of the bottom of the cylinder.

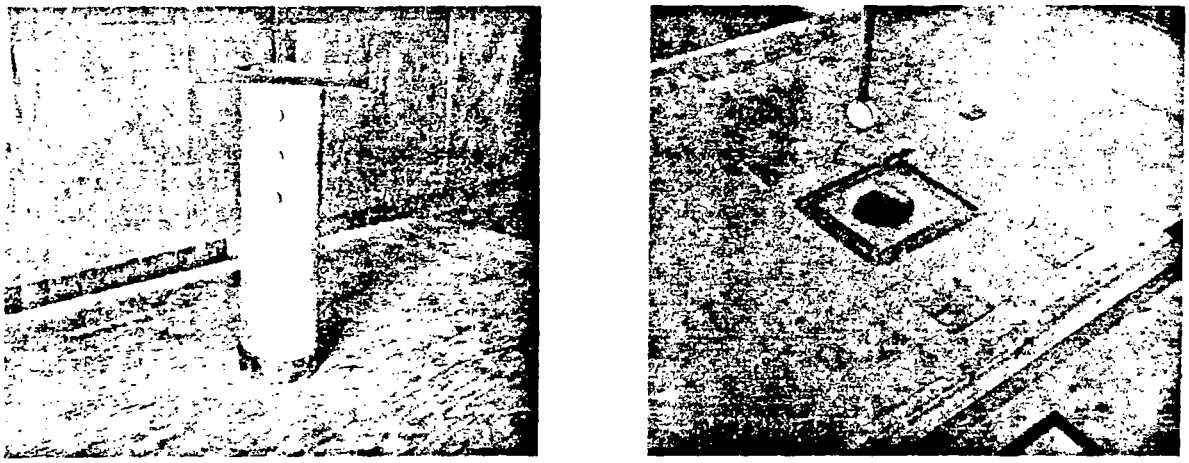

(a) Model Cell

(b) Cell in place with sensor

Figure 11. Missile cell model.

The magnetic field sensor used was a Moebius-strip loop-type[2] constructed from RG-58 cable with a radius of 1 in. The signal was fed into integrators and displayed on a Tektronix 454 oscilloscope housed in a shielded box. The calibration data for the transmission line, with which the measured data were compared, were taken with an EG&G MGL-2 magnetic field sensor. The comparison of the data (fig. 12) indicates that the frequency characteristics of the sensor used for the experiment are equivalent with that of the EG&G sensor, and only an amplitude calibration factor need be applied.

The specific goals of the experimental program were: (1) to verify the exponential decay of the peak amplitude of the field with distance from the cylinder opening, and (2) to justify the quasi-static approximation of the analysis. The first was to be accomplished by measuring the peak field at various distances from the top opening of the opening of the cylinder; the second, by observing that the time history of the pulse inside the cylinder was the same as the time history of the external driving field.

The data were taken with the magnetic field sensor suspended along the axis of the cylinder with the axis of the sensor perpendicular to the axis of the cylinder. In this configuration, the sensor measured the radial component of the magnetic field at three points along the axis of the cylinder (z = 0, 1, and 2 radii) for verification. It was not possible to observe the field farther down the cylinder because of the limited sensitivity of the sensor.

(a)
EG&G MGL-2 SENSOR

50 NS/DIV
200 MV/DIV

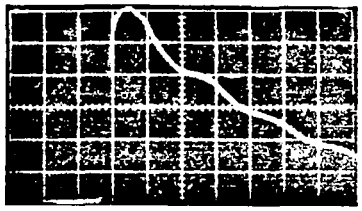

(b)
MOEBIUS LOOP SENSOR

50 NS/DIV
50 MV/DIV

Figure 12. Calibration data for Moebius loop sensor (sensors placed at the center of the transmission line).

[2] Baum, C.E., "Characteristics of the Moebius Strip Loop," EMP Sensor and Simulation Note VII, AFWL, ~~April 1967~~ December 1964.

The oscillographs in figures 13 through 16 show the magnetic fields measured at the three points above with only one section of the cylinder, open at the bottom (fig. 13), one section with closed bottom (fig. 14), two sections with open bottom (fig. 15), and two sections with closed bottom (fig. 16). Apparently, the waveshape is reasonably preserved for all observation points within a given configuration. Also, the observed fields (waveshape) did not vary as the cylinder was lengthened or capped. Figure 17 compares the peak fields observed in this experiment and those predicted by Latham and Lee and shows that the results agree closely.

Thus, Latham and Lee's calculations for the magnetic fields are substantiated by this experimental evidence. Also, this experiment has shown that the quasi-static approximation is reasonable for the geometry considered.

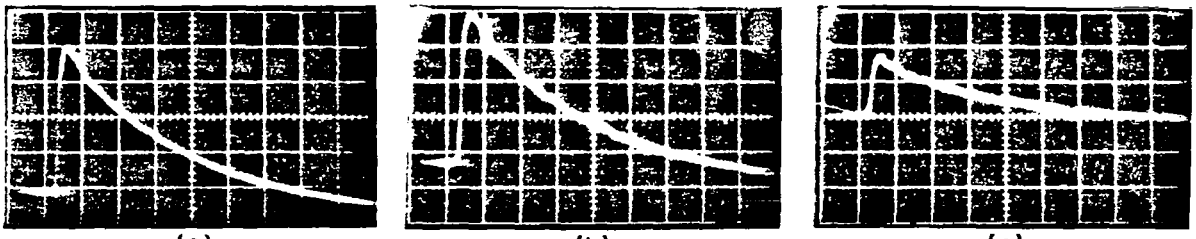

Figure 13. 1 section (24 in.) bottom open.

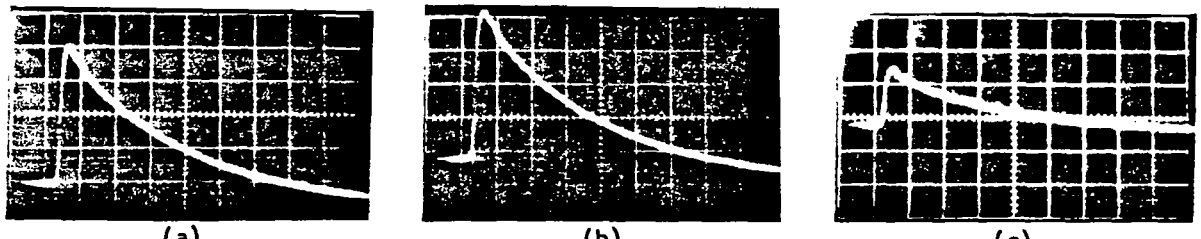

Figure 14. 1 section (24 in.) bottom capped.

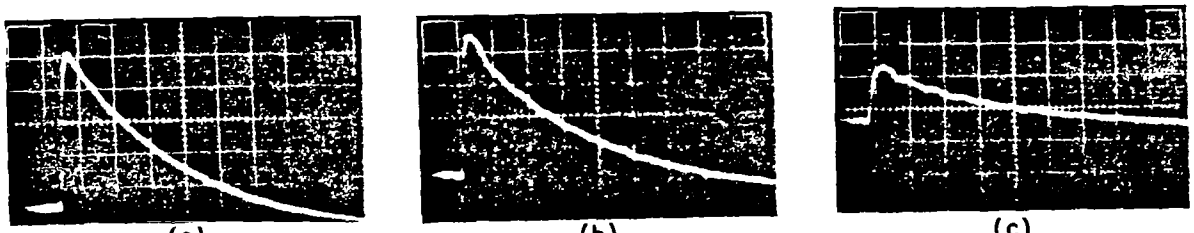

(a)
Z=0

100 NS/DIV
50 MV/DIV

(b)
Z=-3"

100 NS/DIV
10 MV/DIV

(c)
Z=-6"

100 NS/DIV
5 MV/DIV

Figure 15. 2 sections (48 in.) bottom open.

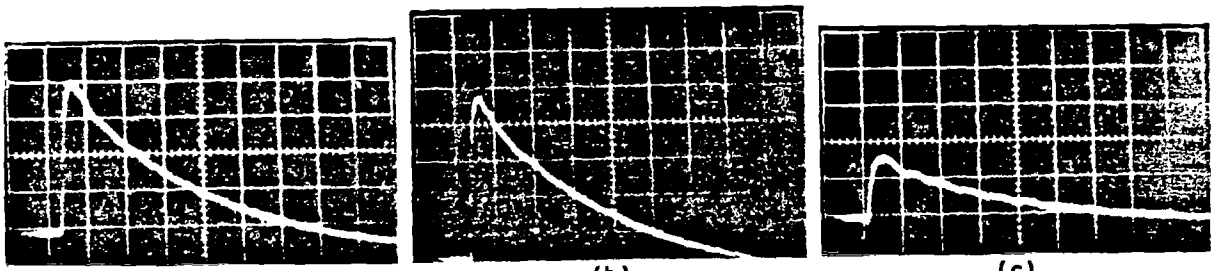

(a)
Z=0

100 NS/DIV
50 MV/DIV

(b)
Z=-3"

100 NS/DIV
10 MV/DIV

(c)
Z=-6"

100 NS/DIV
5 MV/DIV

Figure 16. 2 sections (48 in.) bottom capped.

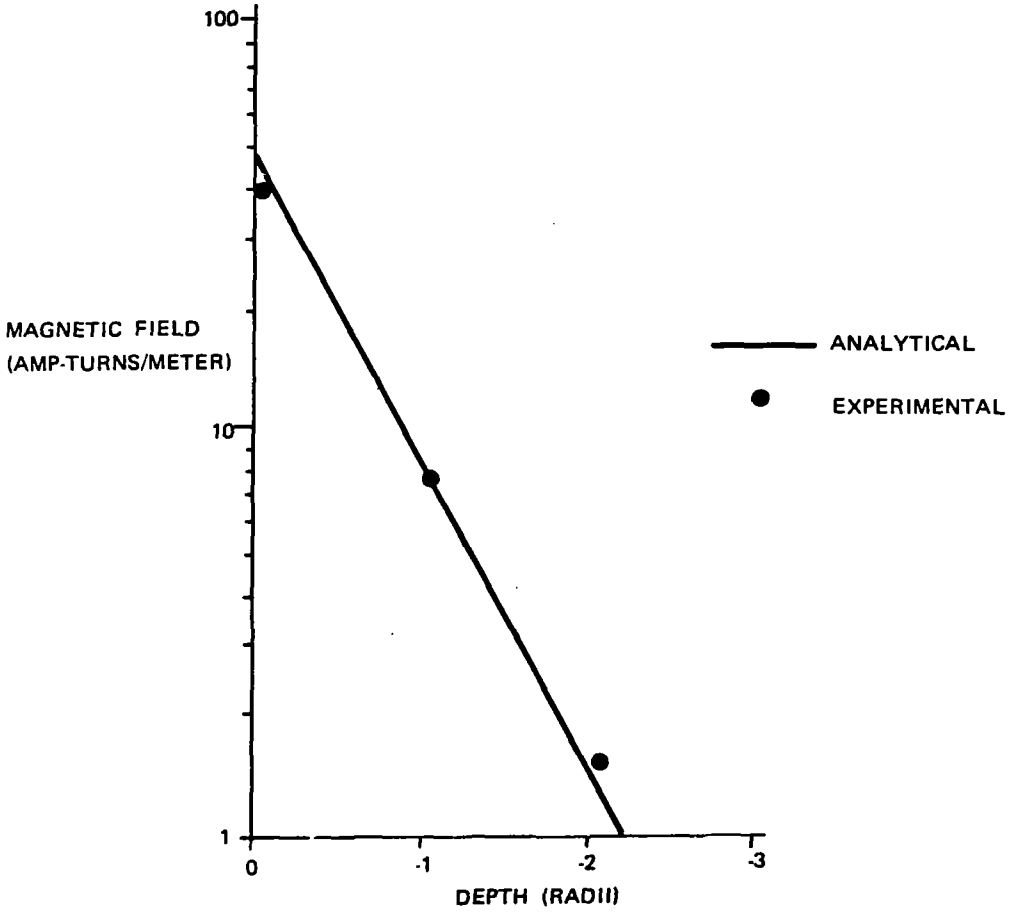

Figure 17. Peak amplitudes of magnetic fields.

DOCUMENT CONTROL DATA - R & D

(Security classification of title, body of abstract and indexing annotation must be entered when the overall report is classified)

1. ORIGINATING ACTIVITY (Corporate author)

Harry Diamond Laboratories
Washington, D.C. 20438

2a. REPORT SECURITY CLASSIFICATION
Unclassified

2b. GROUP

3. REPORT TITLE

MAGNETIC FIELDS INSIDE MISSILE CELL-LIKE STRUCTURES

4. DESCRIPTIVE NOTES (Type of report and inclusive dates)

5. AUTHOR(S) (First name, middle initial, last name)

Daniel J. Spohn

6. REPORT DATE	7a. TOTAL NO. OF PAGES	7b. NO. OF REFS
August 1972	30	2

8a. CONTRACT OR GRANT NO.	9a. ORIGINATOR'S REPORT NUMBER(S)
b. PROJECT NO. MIPR No. 1-01182	HDL-TR-1599
c. AMCMS Code: 5910.21.63389	9b. OTHER REPORT NO(S) (Any other numbers that may be assigned this report)
d. HDL Proj: E01E4	

10. DISTRIBUTION STATEMENT

Approved for public release; distribution unlimited

11. SUPPLEMENTARY NOTES	12. SPONSORING MILITARY ACTIVITY
	U.S. Army Materiel Command

13. ABSTRACT

The analytical work of Latham and Lee describing the static magnetic field inside idealized structures resembling missile cells was reviewed, and a CALCOMP plotting routine was used to graph the results. These results were experimentally verified using a pulsed, parallel-plate transmission line.

DD FORM 1 NOV 68 1473 REPLACES DD FORM 1473, 1 JAN 64, WHICH IS OBSOLETE FOR ARMY USE.

14. KEY WORDS	LINK A		LINK B		LINK C	
	ROLE	WT	ROLE	WT	ROLE	WT
Magneto static fields	8	3				
Flanged cylinder geometry	8	3				